Visualization of mouse kidney perfusion with multispectral optoacoustic tomography (MSOT) at video rate

Andreas Buehler, Eva Herzog, Daniel Razansky and Vasilis Ntziachristos

Institute for Biological and Medical Imaging, Technische Universität München und Helmholtz Zentrum München, Ingoldstädter Landstraße 1, 85764 Neuherberg, Germany

ABSTRACT

Optoacoustic tomography can visualize optical contrast in tissues while capitalizing on the advantages of ultrasound, such as high spatial resolution and fast imaging capabilities. We report herein on a novel multi-spectral optoacoustic tomography system capable of resolving dynamic contrast at video rate and showcase its performance by monitoring kidney perfusion after injection of Indocyaningreen (ICG).

1. KEYWORDS: OPTOACOUSTIC TOMOGRAPHY, MULTISPECTRAL IMAGING, SMALL ANIMAL IMAGING, REAL-TIME IMAGING, KIDNEY IMAGING, MSOTINTRODUCTION

Multispectral optoacoustic tomography (MSOT) is a fast emerging imaging method with the capacity to examine non-invasively structural, physiological and molecular tissue-features in-vivo [1]. The technology is based on the photoacoustic effect, which is the generation of acoustic waves due to thermoelastic expansion of tissue arising from transient temperature increases due to the absorption of nanosecond laser pulses and it combines versatile optical contrast with high scattering-free ultrasonic resolution and is suited for real-time operation.

Optoacoustic imaging has natural sensitivity to haemoglobin being the major absorber of light in tissue. As a consequence, optoacoustic imaging has been employed in the past to resolve vascular contrast changes in superficial tissue [2] and the brain [3]. Later, with the development of multispectral optoacoustic tomography (MSOT), imaging of extrinsic contrast agents such as nanoparticles, fluochromes or other chromophoeres has also been showncased [4-7].

The majority of current small animal optoacoustic imaging systems however utilize scanning configurations that are typically inappropriate for real-time deep tissue small animal imaging. Some of the existing systems scan a single transducer [6, 8-10] around the sample, yielding long acquisition times (minutes to hours). Control of animal physiological parameters, motion and anesthesia during these extended measurement periods can present a significant challenge for obtaining high quality images. Others systems use ultrasound transducer arrays from clinical systems [11, 12] in order to increase the imaging speed, however commercial arrays, optimized for clinical imaging, do not have the geometrical arrangement and broadband frequency characteristics that would make them appropriate for optoacoustic small animal imaging. Additional complications may arise from the use of water coupling, which requires the animal to be fully or partially submerged during the measurement. Dedicated small animal optoacoustic scanners, which utilize high number of detection elements, have also been developed [13, 14]. One of these approaches utilizes a 512 element ring-shaped focused ultrasound transducer array, custom made for small animal imaging, and was successfully applied for anatomical imaging of cerebral blood vessels as well as for imaging of cortical hemodynamics [3, 14]. However, none of these approaches has been so far shown suitable for whole-body small animal visualization in real-time.

We report herein on a new concept for a multispectral optoacoustic tomography (MSOT) scanner for whole body small animal imaging. The scanner utilizes a highly-sensitive concave multielement ultrasound detector array for cross-sectional optoacoustic image formation and optimizes light energy delivery to avoid the need for data averaging.

The design further incorporates an acoustically and optically matched membrane, which allows practical in vivo imaging applications without direct contact between imaged animal and matching transmission medium (water).We characterize

Photons Plus Ultrasound: Imaging and Sensing 2011, edited by Alexander A. Oraevsky, Lihong V. Wang,
Proc. of SPIE Vol. 7899, 789914 · © 2011 SPIE · CCC code: 1605-7422/11/$18 · doi: 10.1117/12.875248

the resolution of the system and showcase its capability to resolve structural, functional and molecular information in small animals in vivo, by monitoring kidney perfusion after the intraveneous injection if Indocyanine Green (ICG).

2. MATERIAL AND METHODS

2.1 System description

An optoacoustic imaging system comprises devices for optoacoustic signal generation, signal detection, signal acquisition, animal positioning and a control and data processing unit. Optoacoustic signal excitation is done with a tuneable (680–950 nm) optical parametric oscillator laser (Phocus, Opotek Inc., Carlsbad, CA), delivering <10ns duration pulses with repetition frequency of 10 Hz. The beam is guided into a silica fused-end fiber bundle (Model PowerLightGuide, CeramOptec GmbH, Bonn, Germany) consisting of 630 fibers partitioned into 10 arms. The arms are separated by 3cm from the animal and create a ring shaped illumination pattern of ~7mm width upon the surface of the animal, coinciding with the ultrasound detection plane. The beam is sufficiently broadened to keep the laser pulse fluence on the surface of imaged objects under 20mJ/cm².

For detection of the optoacoustic signals the system utilizes a custom-made 64 element curved transducer array (Imasonic SaS, Voray, France) covering a solid angle of 172° around the imaged object, as shown in Fig. 1. In this way, it is possible to simultaneously acquire the dataset necessary for a crossectional reconstruction. The individual elements are manufactured using piezocomposite technology with central frequency of 5MHz, bandwidth of more than 50%, and sensitivity of ~18μV/Pa and are shaped in elevation to create a cylindrical focus at 40mm.

The detected optoacoustic signals are digitized at a 60 megasamples/s frequency by eight 12bit multi-channel analog to digital converters (Model PXI5105, National Instruments, Austin, TX) having a noise floor of $\sim 3.8 nV/\sqrt{Hz}$. The data acquisition process is synchronized by the Q-switch trigger of the laser. An embedded controller (NI PXI-8106, National Instruments Corp.) in the same chassis is used for coordinating the instrumentation via a LabVIEW® (National Instruments Corp.) interface.

The animal is held inside a water-impenetrable polyethylene membrane that prevents animal contact with water while providing a wide tomographic view of ~ 180°. The holder also features gas anesthesia supply through a port mounted on one side of the holder where the mouse snout can latch on. A linear stage (NRT150, Thorlabs GmbH, Karlsfeld, Germany) allows linear translation of the holder in the axial z direction over a 150mm range for acquisition of three-dimensional data sets.

As a whole, the acquisition system is capable of acquiring cross-sectional image data at 10 frames-per-second limit imposed by the laser repetition rate.

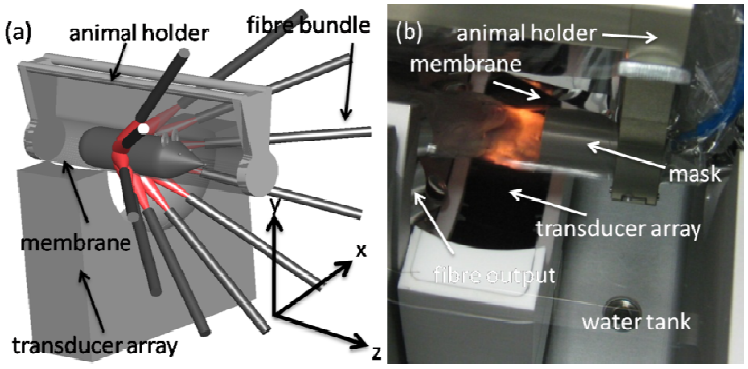

Fig. 1 (a) Schematic representation of the MSOT system. A curved array of wideband and cylindrically focused ultrasound transducers enables parallel data acquisition. Optical fibres are used to homogeneously illuminate the object. A special animal holder with a transparent plastic membrane is used for animal positioning. (b) Picture of a mouse during a scan, showing the position of the mouse and illumination with respect to the array of focused ultrasound transducers.

2.2 Image reconstruction

For the crossectional image reconstruction we employ the interpolated matrix model inversion (IMMI) method [15] which uses an accurate semi-analytical forward model in matrix form

$$\mathbf{p} = \mathbf{M}\mathbf{z} \tag{1}$$

where the photoacoustic signals **p** and the image values **z** are written as column vectors and the matrix M describing the geometry of the imaging system. For inversion of the forward model, we utilized the iterative LSQR algorithm [16], stopping after 50 iterations.

Further, it has to be noted that the reconstructed images **z** do not represent a map of the absorber distribution in tissue but rather a map of the energy deposition, which is the product of local light fluence $U(\vec{r})$ within tissue and the corresponding absorption coefficient $\mu_a(\vec{r})$. Since the photon fluence is heaviliy attenuated as a function of depth, structures deep within the tissue may appear weaker than the same structures close to the animal's surface. Several techniques have been proposed to correct for this inhomogeneous illumination artifacts, including iterative approaches [17] and sparse signal decomposition [18]. In this work we use an analytical normalization [19]

$$U_{norm}(r) = I_0(|k|r) \tag{2}$$

with a modified Bessel function I_0 of the first kind. r stands for the distance from the center of the object in the imaging plane and k for the order.

2.3 Spectral unmixing

Optoacoustic imaging is sensitive to optical absorber contrast. While some highly-concentrated intrinsic chromophores, such as hemoglobin or melanin, can be easily detected in single wavelength images, it becomes challenging to resolve other substances, such as in particular extrinsically administered optical contrast agents over hemoglobin and overall tissue background absorption. In this case multispectral unmixing techniques can improve the image contrast to specific chromphores that attain distinct spectra. Assuming that each pixel in a single wavelength optoacoustic image represents a combined contribution of the probe with the known molar extinction coefficient a_p but unknown concentration c_p and a set of known background absorbers with known spectra a_m and the unknown concentrations c_m (m=1…M), one can define system of linear equations, which takes the form

$$\mu_a(\lambda_n) = a_p(\lambda_n)c_p + \sum_{m=1}^{M} a_m(\lambda_n)c_m, \quad n = 1,...,N \tag{3}$$

where represents one of the N discrete excitation wavelengths. Using the measured absorption and the known spectra, this system of equations can be resolved with linear regression methods in order to reconstruct the probe's biodistribution on a per pixel basis [1][5]. The approach works best when the reporter agents or a substance of interest have a distinct spectral signature over tissue background absorption, as shown for instance in Fig. 4.

2.4 Spatial resolution

The spatial resolution of the system in the imaging plane (in-plane resolution) is limited by the bandwidth and size of the ultrasound detection element. The resolution perpendicular to it (axial resolution) is determined by the width of the focal zone. To measure the spatial resolution experimentally, a 50µm large black microsphere (Cospheric, Santa Barbara, CA, USA) embedded in a small transparent agar cylinder and glued onto the tip of an optical fibre was scanned along a radial line in 1mm steps and in 100µm perpendicular to it. The optoacoustic signals were averaged 10 times to improve the

SNR. The in-plane resolution was determined based on the full width at half maxima (FWHM) of the reconstructed 2D point spread function. The sensitivity field of the transducer arising from its fixed elevation focus was obtained by plotting the magnitude of the optoacoustic signal from the microsphere as a function of its position.

3. RESULTS

3.1 Spatial resolution

Figure. 2 (a) shows the reconstructed 2D point spread function obtained from the 50µm large microsphere in the focal point of the transducer. Its full width at half maxima (FWHM) was used to determine the in-plane resolution. Figure 2(b) shows the in-plane resolution along a radial line as a function of the distance from the transducer element. One can distinguish between radial and lateral resolution. The first describes the extension of the point spread functions along radial line through the center of rotation of the transducer array, the latter the extension perpendicular to it. The radial resolution is limited by the detection bandwidth of the transducer and is constant within the imaging plane. The lateral resolution degrades in the periphery of the imaging plane ranging from the radial resolution in the center to the width of each transducer element in the periphery, which is due to the spatial impulse response of a finite size detector element. Both combined determine the in-plane resolution which is ~150µm in the center of the transducer array. Figure 3 (c) depicts the sensitivity field of the fixed elevation focus which determines the axial resolution. Based on the FWHM one obtains an axial resolution of ~800 µm in the focal point. The focal zone of the transducer is given by the area within which the detection sensitivity drops 6dB. Based on that definition, one obtains a 17mm in diameter large disk shaped imaging domain around the center of rotation of the transducer array, which is appropriate for small animal whole body imaging with target cross-sections in the order of 2cm. Within this imaging domain the systems in-plane resolution is better than 350µm.

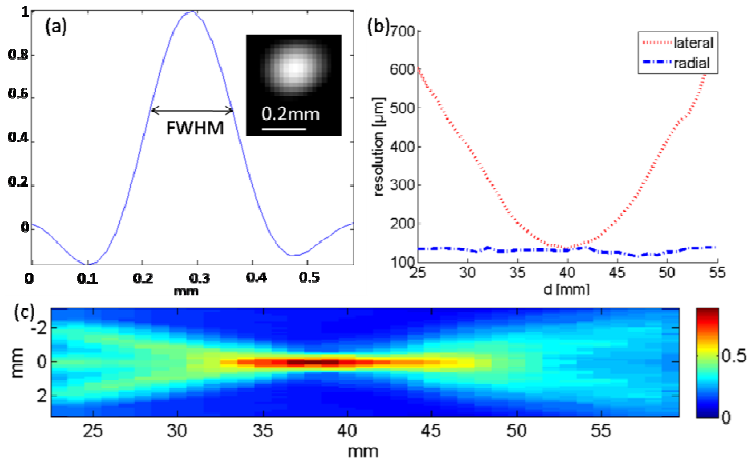

Fig. 2 (a) Profile through a point spread function obtained from reconstructing a 50µm large black microsphere in the imaging plane to determine the in-plane resolution of the imaging system. Inset: crossectional optoacoustic image of the microsphere; (b) In-plane resolution as a function of the distance from the detector. (c) sensitivity field due to the fixed elevation focus.

3.2 Anatomical imaging

Figure 3 shows representative cross-sectional optoacsoutic reconstructions of an adult atymic nude mouse imaged at 850nm. The mouse was positioned in supine position in the animal holder. Signals were preprocessed with a Chebychev bandpassfilter between 50kHz and 7 MHz. The reconstructions were done with the IMMI method on a 200x200 grid

with a pixelsize of 140µm. After reconstruction the Bessel function approach was used to correct for the light attenuation. The reconstructions were also highpass filtered and globally contrast enhanced for better visual perception. There is accurate congruence between features in the non-invasive optoacoustic images and the anatomical photographs of the cryosliced mouse. The abdominal image for instance clearly reveals the kidneys, the spleen, the spine and major vessels like the vena cava. In the thoracic image one could observe the liver with its internal vasculature while the slice made at the head level clearly reveals the outline of the brain with surrounding vessels. Differences observed in the images can be explained by slight organ movements between in-vivo and ex-vivo imaging and differences in the exact height that the in-vivo images and the cryosliced images were acquired from.

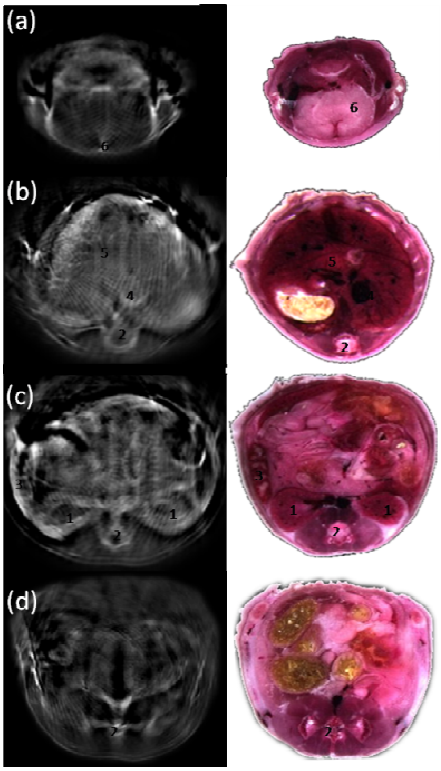

Fig. 3 A selection of crossectional optoacoustic images through the body of a nude atymic CD1 mouse and photographs of corresponding ex-vivo cryoslices. 1-kidneys, 2-spine, 3-spleen, 4-vena cava, 5-liver, 6-brain.

3.3 Imaging of dynamic processes

To showcase the ability of the system to do functional imaging, we imaged mouse kidney perfusion after intraveneous injection of Indocyanene Green (ICG). A female CD1 mouse was anesthetized with a mixture of ketamine and xylazine and hair was removed with a hair removing lotion. The animal was then placed in supine position in the animal holder and 0.3 µmoles of ICG solution were injected into the mouse's tail vein while single-wavelength images were acquired in real-time from the kidney region at 800nm.

Fig.3 shows four selected images of the time-series acquired after ICG injection to show the dynamics of the kidney perfusion. The ICG signal (green) was extracted by substracting the actual image from the image before injection and superimposed on the latter. About 16 seconds after injection of ICG there is the first appearance of ICG in the imaging plane, showing as a localized activity in the center of the image. In the subsequent slices, a gradual spread of the dye into the kidneys can be observed while an increasing number of vascular structures enhance their contrast (optical absorption) due to presence of ICG.

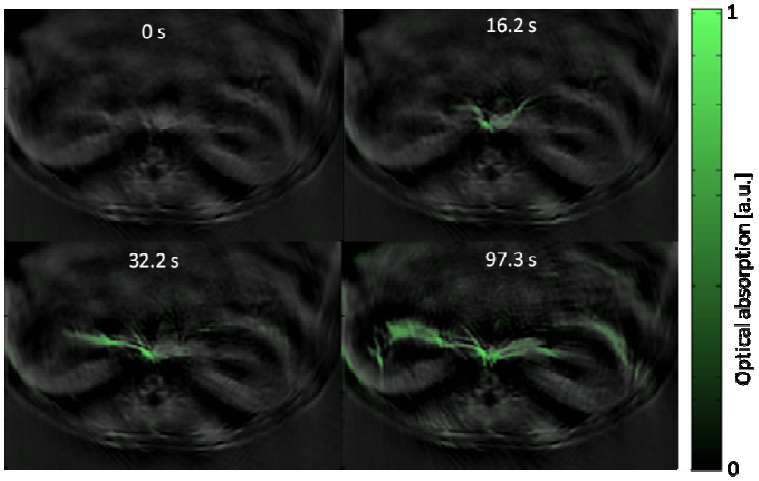

Fig. 4 Crossectional optoacoustic images at different timepoints of the kidneys of a female CD1 mouse illuminated at 800 nm after having injected 0.33µmoles of ICG. The ICG signal (green) was obtained by subtracting the image before injection from the actual one.

3.4 Molecular imaging

Fig. 4 shows the result of MSOT imaging, aiming to investigate whether detection of ICG is possible based on its spectral profile instead of the difference in absorption before and after injection like it was showcased in the previous section. ICG has a characteristic absorption spectrum [21] in the NIR spectral window that differs significantly from the spectra of blood [9] and overall background tissue. For that purpose a multispectral dataset of the kidney was acquired at 5 wavelengths (750nm, 790nm, 810nm, 850nm, 890nm) approximately 3 minutes after injection of ICG. In contrast to perfusion imaging, herein 50 averages were acquired per wavelength. Laserenergy normalization was accomplished utilizing a powermeter (FieldMaxII-TOP with J-50MB-YAG EnergyMax sensor, Coherent Inc., California). After imaging the animal was euthanized. For spectral unmixing, equation (3) was solved by least-square fitting on a per pixel basis using known spectra for ICG, oxygenized and deoxygenized haemoglobin and a constant mock spectrum to intercept remaining spectral components. The image shown is a superposition of the spectrally unmixed image (green) and a single wavelength image at 890 nm showing the relevant anatomical features. Differences in the ICG signal compared to the previous section can be explained by a later time point of the measurement.

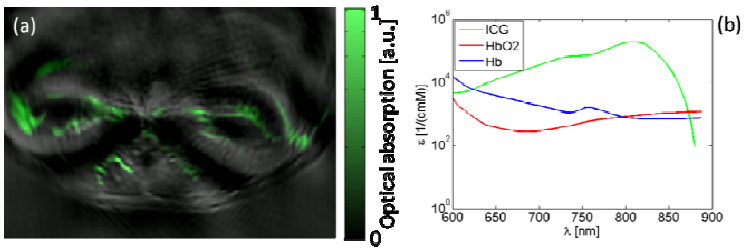

Fig. 5 Superposition of a single wavelength image (890nm) and the unmixed component corresponding to the ICG signal. (b) Molecular extinction coefficient of ICG [20], oxygenized and deoxygenized hemoglobin [7].

4. CONCLUSION

We have developed a novel optoacoustic imaging scanner capable of real-time small animal imaging in-vivo. The system features optimized light energy delivery to avoid the need of data averaging for cross-sectional real-time imaging and provides three dimensional data sets by animal translation along its vertical axis. Further it can acquire optoacoustic data at multiple wavelengths for visualization of structural, functional and molecular contrast with MSOT.

The spatial resolution of the system was measured and yielded in the image center up to 150µm in-plane and up to 800µm in elevation. In the periphery however, there is a degradation of the in-plane resolution which due to the spatial impulse response of the finite size detector element. This issue however can be compensated by adequate modeling of the transducers and is under current research.

Small animal imaging performance was also demonstrated by resolving in real-time mouse anatomy and kidney perfusion using ICG, an exogenously introduced blood-pool agent. Images produced were congruent with corresponding photographs of the mouse anatomy, based on cryoslices obtained from the same animal imaged with MSOT. Spectral unmixing further demonstrated the ability of the system to visualize externally administered contrast based on its unique spectral signature without using background measurements made prior to the probe administration.

In conclusion, the system combines the abilities to image morphological, molecular and functional information in small animals, in and easy to handle and reproducible way and therefore becomes a promising tool for biomedical research.

In the future the system will be used to image other organs and body parts.

5. ACKNOWLEDGMENTS

V.N. acknowledges support from the European Research Council through an Advanced Investigator Award. D.R. acknowledges support from the German Research Foundation (DFG) Research Grant (RA 1848/1).

REFERENCES

1. V. Ntziachristos, and D. Razansky, "Molecular Imaging by Means of Multispectral Optoacoustic Tomography (MSOT)," Chem. Rev. **110**, 2783-2794 (2010).

2. S. Hu, K. Maslov, V. Tsytsarev, and L. V. Wang, "Functional transcranial brain imaging by optical-resolution photoacoustic microscopy," Journal of Biomedical Optics **14** (2009).

3. C. Li, A. Aguirre, J. Gamelin, A. Maurudis, Q. Zhu, and L. V. Wang, "Real-time photoacoustic tomography of cortical hemodynamics in small animals," Journal of biomedical optics letters **15**, 010509 (2010).

4. P. C. Li, C. R. C. Wang, D. B. Shieh, C. W. Wei, C. K. Liao, C. Poe, S. Jhan, A. A. Ding, and Y. N. Wu, "In vivo Photoacoustic Molecular Imaging with Simultaneous Multiple Selective Targeting Using Antibody-Conjugated Gold Nanorods," Optics Express **16**, 18605-18615 (2008).

5. D. Razansky, J. Baeten, and V. Ntziachristos, "Sensitivity of molecular target detection by multispectral optoacoustic tomography (MSOT)," Med. Phys. **36**, 939-945 (2009).

6. D. Razansky, M. Distel, C. Vinegoni, R. Ma, N. Perrimon, R. W. Koster, and V. Ntziachristos, "Multispectral opto-acoustic tomography of deep-seated fluorescent proteins in vivo," Nat. Photonics **3**, 412-417 (2009).

7. A. Taruttis, E. Herzog, D. Razansky, and V. Ntziachristos, "Real-time imaging of cardiovascular dynamics and circulating gold nanorods with multispectral optoacoustic tomography," Optics Express **18**, 19592-19602.

8. R. Ma, A. Taruttis, V. Ntziachristos, and D. Razansky, "Multispectral optoacoustic tomography (MSOT) scanner for whole-body small animal imaging," Optics Express **17**, 21414-21426 (2009).
9. D. Razansky, C. Vinegoni, and V. Ntziachristos, "Multispectral photoacoustic imaging of fluorochromes in small animals," Optics Letters **32**, 2891-2893 (2007).
10. X. D. Wang, Y. J. Pang, G. Ku, X. Y. Xie, G. Stoica, and L. H. V. Wang, "Noninvasive laser-induced photoacoustic tomography for structural and functional in vivo imaging of the brain," Nature Biotechnology **21**, 803-806 (2003).
11. S. A. Ermilov, T. Khamapirad, A. Conjusteau, M. H. Leonard, R. Lacewell, K. Mehta, T. Miller, and A. A. Oraevsky, "Laser optoacoustic imaging system for detection of breast cancer," Journal of Biomedical Optics **14**, 024007 (2009).
12. B. Z. Yin, D. Xing, Y. Wang, Y. G. Zeng, Y. G. Zeng, Y. Tan, and Q. Chen, "Fast photoacoustic imaging system based on 320-element linear transducer array," Phys. Med. Biol. **49**, 1339-1346 (2004).
13. H. P. Brecht, R. Su, M. Fronheiser, S. A. Ermilov, A. Conjusteau, and A. A. Oraevsky, "Whole-body three-dimensional optoacoustic tomography system for small animals," Journal of Biomedical Optics **14**, 064007 (2009).
14. J. Gamelin, A. Maurudis, A. Aguirre, F. Huang, P. Y. Guo, L. V. Wang, and Q. Zhu, "A real-time photoacoustic tomography system for small animals," Optics Express **17**, 10489-10498 (2009).
15. A. Rosenthal, D. Razansky, and V. Ntziachristos, "Fast semi-analytical model-based acoustic inversion for quantitative optoacoustic tomography," IEEE Transactions on Medical Imaging **28**, 1997 - 2006 (2010).
16. C. C. Paige, and M. A. Saunders, "Lsqr - an Algorithm for Sparse Linear-Equations and Sparse Least-Squares," Acm Transactions on Mathematical Software **8**, 43-71 (1982).
17. T. Jetzfellner, D. Razansky, A. Rosenthal, R. Schulz, K. H. Englmeier, and V. Ntziachristos, "Performance of iterative optoacoustic tomography with experimental data," Appl. Phys. Lett. **95** (2009).
18. A. Rosenthal, D. Razansky, and V. Ntziachristos, "Quantitative optoacoustic signal extraction using sparse signal representation," IEEE Trans Med Imaging **28**, 1997-2006 (2009).
19. D. Razansky, and V. Ntziachristos, "Hybrid photoacoustic fluorescence molecular tomography using finite-element-based inversion," Med. Phys. **34**, 4293-4301 (2007).
20. M. H. Xu, and L. H. V. Wang, "Universal back-projection algorithm for photoacoustic computed tomography," Phys. Rev. E **71** (2005).
21. M. L. J. Landsman, G. Kwant, G. A. Mook, and W. G. Zijlstra, "Light-Absorbing Properties, Stability, and Spectral Stabilization of Indocyanine Green," Journal of Applied Physiology **40**, 575-583 (1976).